APPLICATION OF SHJ AND TOPCON SHINGLE CELLS IN FULL FORMAT AND INTEGRATED MODULES

V. Nikitina[1], D. Reinwand[1], T. Fellmeth[1], S. Neven du Mont[1], D. v. Kutzleben[1], T. Roessler[1], D. H. Neuhaus[1]
[1]Fraunhofer Institute for Solar Energy Systems (ISE)
Heidenhofstr. 2, 79110 Freiburg, Germany

ABSTRACT: Shingle technology is attractive due to the absence of ribbons or wires, large active module area, module design flexibility and aesthetically appealing appearance [1]. This work is looking into the application of silicon heterojunction (SHJ) and tunnel oxide passivated contact (TOPCon) shingle cells in small-scale and full-format modules as well as into the effects of overlap minimization and electrically conductive adhesive (ECA) reduction. Stringer tests with subsequent microscopic analysis showed that precision of the laser cutting process is crucial for the correct alignment of metallization and ECA during the interconnection process. Shunting as well as ECA smearing can be caused by the inconsistent distance of the metallization to the cell edge. The variation of the ECA, printing pattern and encapsulation material in small-scale modules demonstrated no difference in performance after production. However, after accelerated thermal cycling (aTC) 50 the modules with SHJ cells showed $\Delta P_{MPP} = -8.2\%_{rel}$ to $+0.4\%_{rel}$, and TOPCon between $-4.5\%_{rel}$ and $+0.6\%_{rel,}$ depending on the used encapsulation material. No difference in performance for the modules with reduced ECA amount in comparison with the reference was detected after aTC50. Full-size solar modules with bifacial TOPCon shingles (1/6 G1 format, 20.7% − 21.3% efficiency after the scribe and break laser process) were manufactured with 50% ECA reduction and the optimal materials based on the previous investigation. Peak power values of up to 392.8 Wp and Eta of 19.84% were demonstrated.

Keywords: PV Modules, Shingling, Heterojunction, TOPCon, Electrically Conductive Adhesive (ECA)

1 INTRODUCTION

Using shingle technology enables creating solar modules of flexible shapes and sizes, which is crucial for the field of integrated photovoltaics. Residential and solar park applications also profit from shingling technology due to the homogeneous appearance of the modules and their large active area [2]. Improved shading resilience of the shingle technology compared to ribbon interconnection is advantageous in all usage scenarios [3]. By reducing the amount of the silver containing electrically conductive adhesive (ECA) in a shingle module, the total cost can be significantly reduced. Carriere et al. demonstrated neither influence on cell-to-module (CTM) loss nor reliability when reducing the ECA amount with silicon heterojunction (SHJ) shingle cells [4]. In this work we investigate the interconnection of SHJ and tunnel oxide passivated contact (TOPCon) cells by shingle technology, targeting full-size and vehicle integrated photovoltaic (VIPV) module production. We aim to cut down the ECA amount as well as maximize the silicon usage by reducing the shingle overlap.

2 METHODS

2.1 Approach

In order to address the issues of shingle overlap minimization, ECA reduction and full-format module integration, a range of experiments was conducted. We investigated the effect of the overlap on the interconnection quality and factors affecting shingle placement precision on a teamtechnik TT1600ECA stringer. The potential to reduce ECA amount as well as different ECAs and encapsulation materials were examined with small-scale modules. The samples were subjected to accelerated thermocycling (aTC) tests [5]. After the most promising material combination had been determined, full-format TOPCon shingle modules were produced. Additionally, a car hood module concept was developed and realized. Evaluation of the string and module performance was done by electroluminescence (EL) and I-V measurements. Metallographic analysis with digital microscopy was used for the shingle overlap investigations. Determination of the series resistance was done according to the procedure described in IEC60891 [6]. Furthermore, Magnetic Field Imaging (MFI) was utilized to look into the terminal connector defects [7].

2.2 Microscopy

A TT1600ECA stringer upgraded for automatic shingle interconnection allows varying overlap in the range of 0.5 mm to 5 mm. Samples for the investigation of overlap reduction were produced on the stringer with the set value of 0.8 mm. Experiments were performed with SHJ shingles, for which the screen design matching with the metallization pads was used. Both front and rear side metallization included rectangular pads every second finger (fig. 1). ECA was applied by screen printing in such a way that every finger-busbar intersection is covered with an ECA rectangle equal to the metallization pad size (0.4 mm × 0.7 mm with 1.4 mm distance, 3.8 mg (ECA-II)). In addition to planar microscopy of the ECA print over the metallization, cross-sections of the joints were prepared according to the procedure described by Eberlein et al [8].

2.3 Fabrication of small-scale modules

Analysis of the small-scale modules was done to obtain the optimal material combination for further full-size module production. Small-scale modules were produced according to the variation in table I with SHJ and TOPCon shingles, respectively. Both shingle types were in 1/6 G1 format (158.75 mm × 26.46 mm). For the TOPCon cells, the metallization of the industrial bifacial precursors was realized at Fraunhofer ISE, using Ag paste for busbars, AgAl paste for front side fingers and Ag paste for the back side fingers. The performance of the shingles after the laser scribe and break process was 20.7% − 21.3% Eta and 0.86 – 0.88 W, measured with pins on the busbars on each side, respectively. For the bifacial

SHJ shingles a low-temperature Ag-based metallization paste with a special print design with reduced paste consumption was used (fig. 1). The cells were cut with laser scribe and break process as well and had efficiency range of 18.4% − 19.0% and P_{MPP} range of 0.78 W – 0.80 W, measured with universal contact probes (UCP) after cutting, respectively.

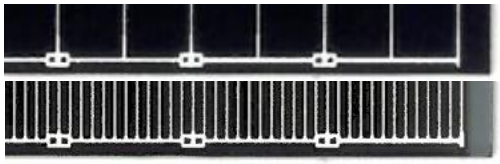

Figure 1: Metallization design on SHJ shingle cells used in this work. Upper – front side, lower – rear side.

Three different ECAs were tested with both cell types: ECA-I (Ag filled acrylate, density 1.9 g/cm^3), ECA-II (Ag and Cu filled epoxy, density 4.0 g/cm^3) and ECA-III (Ag filled epoxy, density 2.0 g/cm^3). For the small-scale modules the adhesives were applied manually as a continuous line of 0.2 mm and as a pad pattern (0.3 mm × 0.5 mm with 0.6 mm distance) through a stencil with 100 µm thickness. The pad design leads down to half of the ECA weight in comparison to the continuous one: 2.5 ± 0.3 (SE) mg vs. 4.8 ± 0.6 mg (measured with ECA-I). The produced small-scale strings (six shingles in a sequence with 1.1 mm overlap) were laminated with polyolefin encapsulation materials from two different manufacturers: PO-I and PO-II. The small-scale modules were laminated in a glass-glass design in a 200 mm × 200 mm size. The glass thickness was 3.2 mm.

Table I: Small-scale module variation. Such sample matrix was used for the SHJ and TOPCon group, respectively; "continuous" and "pads" describe ECA application pattern; "PO-I" and "PO-II" are two types of encapsulation material.

ECA-I				ECA-II		ECA-III	
continuous		pads		pads		pads	
PO-I	PO-II	PO-I	PO-II	PO-I	PO-II	PO-I	PO-II

2.4 Full-size and VIPV module production

With the material choice based on the results of the small-scale module testing, full-format modules (1960 mm × 1010 mm × 2 mm) in glass-glass design with 12 strings 38 shingles each (6 strings in parallel) were produced. Full-size module fabrication was realized with TOPCon shingle cells, ECA-II and PO-I. The TT1600ECA stringer was utilized for the interconnection. The machine used screen printing to apply ECA-II in a pad pattern (4.8 mg per shingle, note the higher density of ECA-II compared to ECA-I). The robot arm system ensured an automatic shingle placement with 1.1 mm overlap, based on the metallization design of the TOPCon shingles (busbar width and position relative to the cell edge). Lamination took place in a Bürkle Ypsator laminator with a 3-step process: plate-membrane (150 °C, 7.5 min), followed by plate-plate (150 °C, 7.5 min) and finishing in cooling press (20 °C).

The vehicle integrated modules in this work (i.e. car bonnets) required an individual solution when it came to material choice and lamination due to their curved shape and metal substrate. The lamination of the bonnet took place in a Bürkle 3D laminator with a custom aluminum negative form. In order to electrically isolate the bonnet and the module, black insulation layer was used. For the VIPV modules, TOPCon shingle cells were interconnected analogically to the strings for the conventional full-size modules. One bonnet module comprised five strings, 30 shingles each, connected in parallel.

2.5 Module testing and characterization

After production, the small-scale modules were measured and compared in terms of *I-V* parameters and uniformity of the electroluminescence (EL) signal. Series resistance was calculated based on the *I-V* curve. Then, the small-scale modules were tested in an accelerated thermocycling (aTC) chamber with 50 cycles followed by 150 cycles. The sample degradation was analyzed. The aTC procedure differs from the thermocycling (TC) testing as described in IEC61215 [9] by the absence of current surge and the use of six times quicker temperature ramps (8 K/min, T_{max} = 85°C, T_{min} = −40°C). This allows identifying differences in the degradation behavior between groups in a short period of time. In order to gain understanding in possible terminal connector defects, Magnetic Field Imaging (MFI) was used.

3 RESULTS

3.1 Microscopic analysis of shingle interconnection

Three principal types of joints were identified during the investigation of the strings with 0.8 mm overlap. Figure 2a shows an ECA printing offset, which is caused by poor screen alignment and can be avoided with an adjustment during production. The second case (fig. 2b) depicts a lower distance from metallization to the shingle edge, causing shunting of the string and negatively affecting the string appearance due to ECA smearing. This can be solved by enhancing the precision of the laser cutting process. Fluctuating distance from the edge to the busbar as a result of unprecise cutting makes it difficult to set up a stable alignment of ECA print and metallization while keeping a constant physical overlap less than 1 mm. Figure 2c demonstrates correct ECA print directly over the metallization pad and precise placement of the shingles above one another creating a shortest possible current path between the shingles.

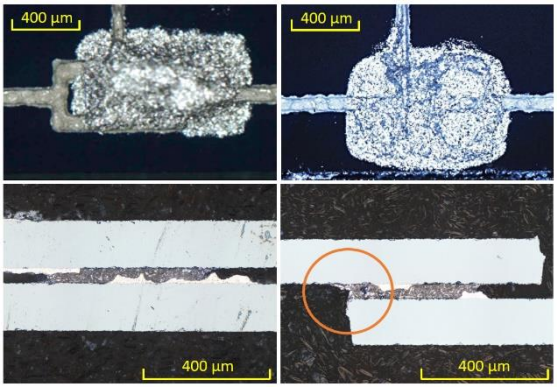

(a) (b)

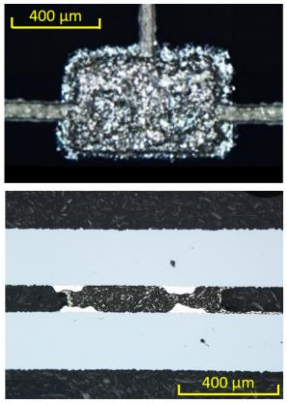

(c)

Figure 2: Top – planar microscopic images of the metallization sections of the SHJ busbar area with printed ECA pads. ECA pad dimensions: 0.7 mm × 0.4 mm. Bottom – cross-sections of the corresponding situations in the shingle joint. (a) ECA is printed with an offset to the cell metallization. (b) Due to the unprecise cutting, the ECA is too close to the edge causing shunting (orange circle). (c) ECA is printed correctly as well as shingles placed precisely, so that metallization of the upper cell lays directly above the metallization of the lower cell with ECA in between.

3.2 ECA reduction and module material optimization

Based on the *I-V* measurement after production (tab. II), no material- or design-dependent differences in the performance of the small-scale modules (fig. 3) were observed.

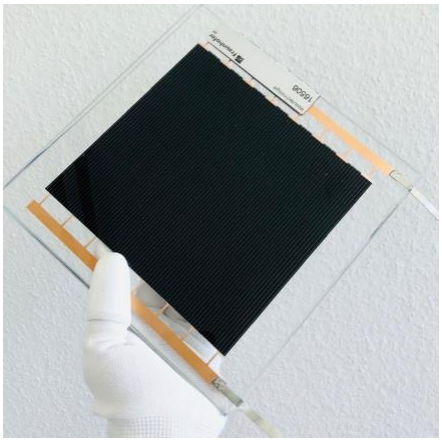

Figure 3: Small-scale module. Six shingles interconnected in a sequence with a copper terminal connector on each side. Terminal connectors are extended with SnPb-coated bussing ribbons.

Table II: Mean values of the *I-V* parameters of the small-scale modules after lamination.

	V_{OC}	I_{SC}	*FF*	P_{MPP}
SHJ with PO-I	4.4 V ±0.1%*	1.4 A ±1.4%	77.1 % ±1.5%	4.9 W ±1.8%
SHJ with PO-II	4.4 V ±0.1%	1.4 A ±1.2%	77.1 % ±1.5%	4.9 W ±2.0%
TOPCon with PO-I	4.2 V ±0.1%	1.6 A ±0.8%	78.4 % ±0.7%	5.2 W ±0.5%
TOPCon with PO-II	4.2 V ±0.1%	1.6 A ±3.6%	78.5 % ±1.7%	5.2 W ±2.3%

* standard error (SE)

After the aTC50 test, the small-scale modules were measured again and the loss in *I-V* parameters relative to the initial values was calculated (fig. 4). V_{OC} demonstrated no difference in TOPCon samples, whereas SHJ samples showed average −3.4%$_{rel}$ across all groups. We do not assume this to be an effect of the shingle interconnection or module fabrication but an instability of the cell itself. I_{SC} is slightly increased for TOPCon (+0.2%$_{rel}$) and fluctuates around zero change for SHJ. In both cell groups *FF* and P_{MPP} show strong correlation after aTC50, which implies same governing factors, which in this case is increasing series resistance. TOPCon samples demonstrate no to slight (−0.5%$_{rel}$) *FF* or P_{MPP} loss with PO-II whereas PO-I causes up to −4.5%$_{rel}$ ΔP_{MPP} and −4.8%$_{rel}$ ΔFF due to string corner breakage (fig. 5) with a strong scattering of the values (fig. 4, green hollow triangles). Usage of a 3.2 mm thick glass for small-scale modules in combination with 450 µm encapsulation material likely causes such an effect. Based on experience with thinner glass (2 mm, as used in full-format modules) no breakage for lower glass-POE thickness ratio is expected.

Within the SHJ group, an overall increase in *FF* of up to +4.1% is to be seen. ΔP_{MPP} is dispersed between −8.2%$_{rel}$ and +0.4%$_{rel}$, with the majority of the small-scale modules showing no to moderate (−2.0%$_{rel}$) degradation (Fig. 4, orange hollow circles). Extreme values in this case were caused by the partial detachment of the terminal connectors (not depicted in fig. 4) and degradation around the crack already present after lamination.

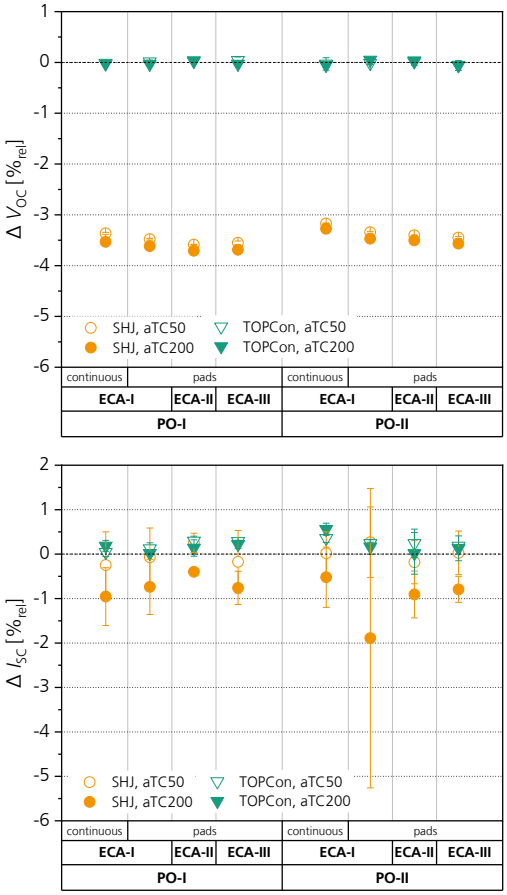

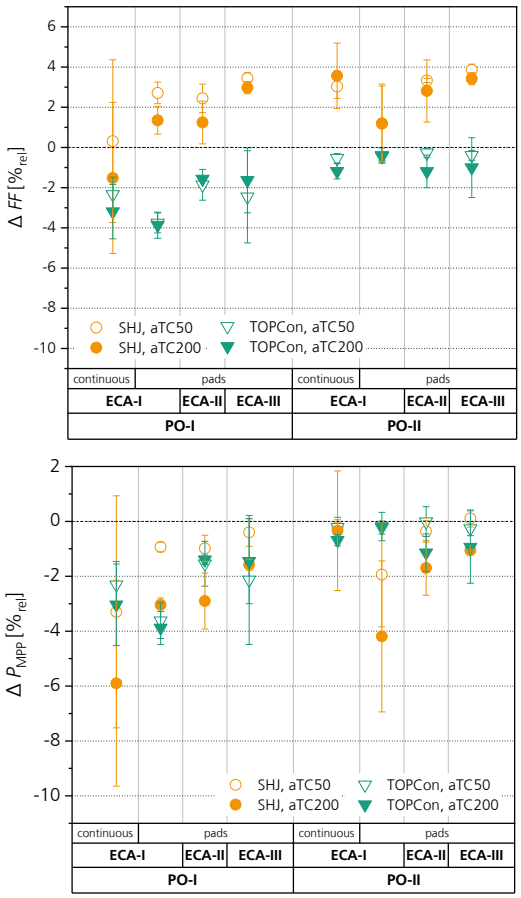

Figure 4: Relative loss in (from top to bottom) V_{OC}, I_{SC}, *FF* and P_{MPP} of small-scale modules as a result of aTC50 and aTC200 tests. Mean of three samples per variation is plotted, error bar – standard error (SE). Zero level - initial *I-V* characteristics (after lamination). "PO" – encapsulation material, "ECA" – conductive adhesive, "continuous" and "pads" – adhesive printing patterns.

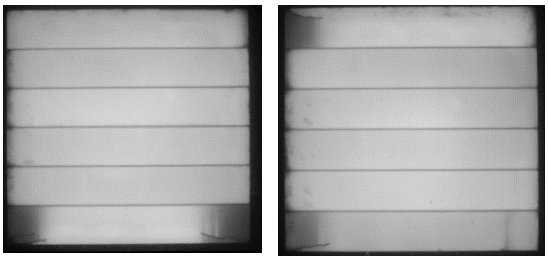

Figure 5: EL images of the small-scale modules with edge string breakage. Measurement setup: current = 3 A, exposure time = 600 ms.

As a result of further 150 cycles in the aTC test, TOPCon modules with PO-II demonstrate stronger degradation than after 50 cycles, whereas samples fabricated with PO-I either keep the same degradation or slightly gain P_{MPP} (fig. 4). Increase in P_{MPP} occurs with the ECA-III most likely due to further curing within the module when exposed to high temperatures (during aTC testing up to 85°C). This is confirmed by the reduced R_S after aTC200 for this adhesive (fig. 6, blue triangles). Similarly to aTC50, Δ*FF* strongly correlates with ΔP_{MPP}. V_{OC} shows no change after aTC200 in comparison to aTC50. I_{SC} for the samples with continuous print gained up to 0.3%$_{rel}$, whereas ΔI_{SC} for samples with pad application with the same ECA counts +0.1%$_{rel}$ to −0.2%$_{rel}$.

Small-scale modules with SHJ shingles show further V_{OC} decrease across all groups by 0.15%$_{rel}$, which can be attributed to further cell degradation after aTC200. I_{SC} demonstrates 0.3%$_{rel}$ to 2.0%$_{rel}$ lower values in all variations with no trends. ΔI_{SC} correlates with ΔP_{MPP} in samples with PO-II, which is an indication of encapsulation material degradation and its negative effect on the peak power. While ΔP_{MPP} in samples with PO-II is mostly governed by the encapsulation material degradation, P_{MPP} loss in small-scale modules with PO-I are affected by *FF* loss. Δ*FF* with SHJ samples after aTC200 produced with PO-I shows the most dependency on the R_S. Samples with PO-II show less change in Δ*FF* values, due to allegedly less thermomechanical stress, affecting the interconnection.

The series resistance R_S, mostly ranging from 0.1 Ω to 0.3 Ω is slightly different for SHJ (fig. 6, above) and for TOPCon (fig. 6, below) cells. Initial mean R_S values with TOPCon cells are overall lower (0.11 ± 0.03 (SE)) Ω, than with SHJ cells (0.14 ± 0.05) Ω. A comparison of the initial values between the full (continuous) and reduced (pad) ECA application with ECA-I shows that TOPCon cells are robust against the ECA reduction; there is hardly any difference visible (fig. 6, orange triangles). SHJ cells in this case demonstrate a large scattering of the values for the pad ECA application design (orange circles). This indicates that the special metallization design of the SHJ shingles (fig. 1) is sensitive to ECA reduction at least with this particular adhesive. Further reduction of the ECA-I amount on such metallization design may cause worse module performance and reliability. After aTC50 the overall increase in R_S can be observed. Again, TOPCon shingles showed generally better results with average increase by (0.03 ± 0.03) Ω, whereas with SHJ it measured (0.04 ± 0.05) Ω. After aTC200 change in R_s is substantially lower for both cell types: (0.008 ± 0.020) Ω for TOPCon and (0.004 ± 0.026) Ω for SHJ. ECA-II together with TOPCon cells (fig. 6, bottom, middle section) is the best performing combination in terms of R_S values and interconnection stability (data scattering).

Overall, series resistance increase caused by joint degradation and short circuit current loss due to encapsulation degradation are the main causes for the performance loss in small-scale modules. Both of these effects can be avoided if a right material combination (ECA type, ECA application amount, encapsulation type) is used.

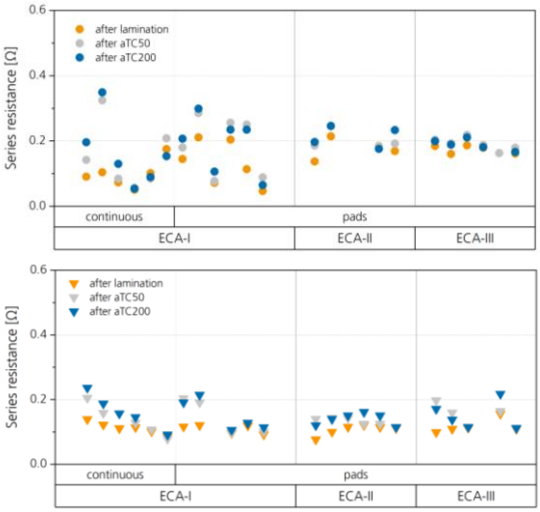

Figure 6: Series resistance of small-scale SHJ (top) and TOPCon (bottom) modules after lamination (orange), aTC50 (grey) and aTC200 (blue). "ECA" – conductive adhesive, "continuous" and "pads" – adhesive printing patterns. Samples with PO-I and PO-II of the same interconnection group are considered together.

Moreover, dendric-shaped features appear in a number of modules with PO-II after aTC200, indicating failure of the encapsulant possibly because of its partial melting and recrystallization (fig. 7).

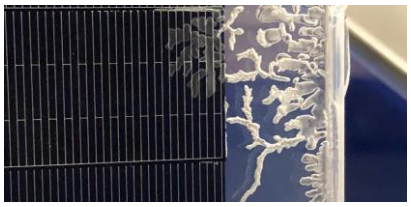

Figure 7: Features in encapsulation material abundant with PO-II samples after aTC200.

3.3 Terminal connection

Two small-scale modules with SHJ cells demonstrated unusually high losses after aTC50 (−14.2%$_{rel}$ ΔP_{MPP} (fig. 8, first row) and −4.8%$_{rel}$ ΔP_{MPP} (fig. 8, second row)) while EL images (Fig. 8, left) indicated no breakage but darkening of the whole string with local overexposure in the first cell. MFI images (Fig. 8, right) demonstrated uneven current flow distribution on one pole of each sample, matching with the EL signal. The bottom edge pattern of the MFI images correlates with the positioning of the terminal connector, whereas the current flow on the top is localized in one spot. The busbar of the SHJ cells is more sensitive to terminal connector misplacement or movement during module production than a full busbar metallization design. Visual inspection of the modules confirms the faulty positioning (fig 8, below). Since the data indicates defects in terminal connection, whereas the cell connection within the string appears homogeneous, these samples were not considered in the section 3.2.

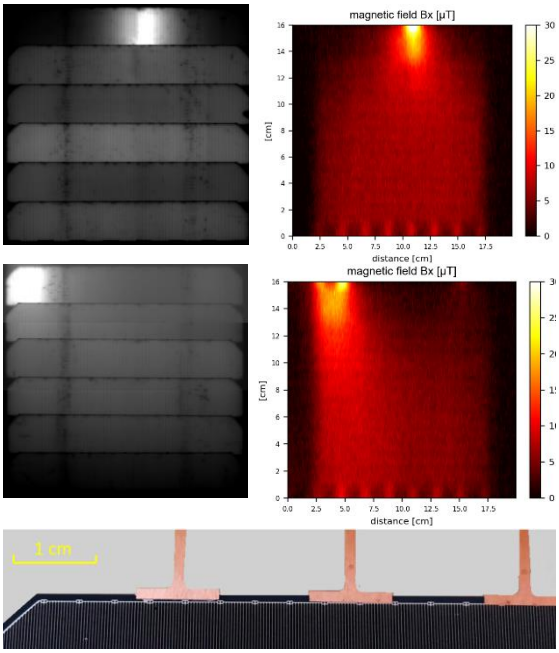

Figure 8: Left – EL images of SHJ small-scale modules with terminal connector defects. EL setup: 0.14 A, 2000 ms. Right – dark MFI of the corresponding samples. MFI setup: 1.7 A. All measurements taken after aTC50. Bottom – photo of the terminal connector defect area.

3.4 Full-format and integrated modules

Based on the results of the small-scale module testing and gained understanding of the degradation behavior of the material combinations an optimal set of TOPCon shingles, ECA-II with pad application and PO-I was chosen for the full-format module production. Three full-format modules were fabricated in a glass-glass configuration. They demonstrated P_{MPP} values of 389.7 W (fig. 9a), 392.8 W (fig. 9b) and 376.8 W (fig. 9c), and full area efficiencies of 19.68%, 19.84% and 19.04%, respectively. This attributes to a CTM of −2.2%$_{rel}$ to −6.3%$_{rel}$ in ΔP_{MPP} and −8.4%$_{rel}$ to −12.3%$_{rel}$ $\Delta\eta$ (fig. 10). The main portion is related to a loss in short circuit current due to cell shading as a result of overlap. EL images indicate no major defects and homogeneous interconnection.

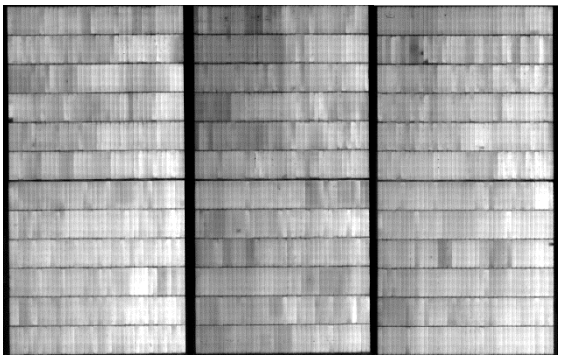

(a) (b) (c)

Figure 9: EL images of the full-format TOPCon modules. Measurement setup: current = 10 A, exposure time = 2000 ms.

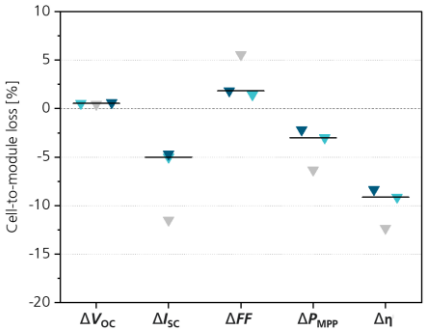

Figure 10: Change of the key *I-V* parameters after the full-format module lamination. Each color depicts one module from fig. 12: cyan – (a), navy – (b), grey – (c).

A prototype of a car bonnet module for Volkswagen Polo was successfully manufactured (fig. 11). Further details to the prototype will be described in in a separate publication and are briefly mentioned in Tous et al. [10]. Such module can serve as a power source in addition to a solar integrated car roof. Another advantage of a solar bonnet is the possibility to upgrade already assembled cars due to the relatively easy bonnet part extraction.

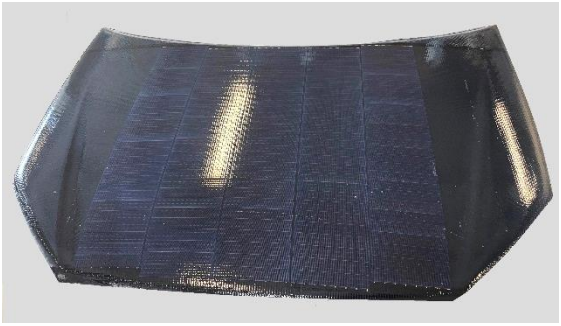

Figure 11: Car bonnet with an integrated solar module developed and produced at Fraunhofer ISE.

4 CONCLUSIONS AND OUTLOOK

4.1 Conclusions

By investigating shingle joints with 0.8 mm overlap, current study demonstrates that reliable interconnection with overlap under 1.0 mm cannot be realized with unprecise cutting, because the metallization print and ECA are too close to the cell edge and may cause shunting.

Based on the small-scale module production and testing with an aTC procedure, following can be concluded. Samples with PO-I after aTC50 show abundant cell breakage. Such breakage is most likely caused by the too low glass-PO thickness ratio and overlay the influence of the ECA. PO-II systematically demonstrates visible defects after aTC200 possibly caused by melting and recrystallization of the polymer. Series resistance of the small-scale modules showed that TOPCon cells with their full busbar have initially lower R_S (0.11 ± 0.03 Ω) and are more robust against ECA amount reduction and aTC testing (increase by 0.03 ± 0.03 Ω) than SHJ shingles (0.14 ± 0.05 Ω and 0.04 ± 0.05 Ω, respectively). ECA amount reduction by down to 50% does not result in lower *I-V* values neither after the module production nor after aTC. The terminal connection is a critical process that can lead to significant CTM and reliability losses and must be optimized. TOPCon cells interconnected with ECA-II (reduced amount) and laminated with PO-I is the best performing combination after aTC200 (fig. 4. 6).
Full-format glass-glass TOPCon shingle modules were produced and demonstrated P_{MPP} up to 392.8 W with the highest efficiency of 19.84%.

4.2 Outlook

The reduced ECA application design used in this work shows great potential for silver saving, making shingle technology cheaper. Tests according to IEC protocols will be conducted at Fraunhofer ISE in the framework of other projects to demonstrate reliability of shingle interconnection with this application design.

Further optimization work on the shingle string terminal connector is yet to be done. While metallization layouts with wide busbars seem to withstand stress of the reliability tests, metallization paste reduction in the busbar area of the shingle cells requires more robust solutions.

ACKNOWLEDGEMENTS

Current study was prepared in the framework of the project HighLite, which was funded by the European Union's Horizon2020 Programme under Grant Agreement No 857793.

REFERENCES

[1] M. Mittag et al, *Proceedings of the 44th IEEE*, p. 1531–1536 (2017).
[2] T. Rößler, et al, *AIP Conference Proceedings*, accepted (2022).
[3] N. Klasen et al, *IEEE Journal of Photovoltaics*, Vol. 12–2, p. 546–556 (2022).
[4] C. Carriere et al, *Proceedings of the 37th EUPVSEC*, p. 840–844 (2020).
[5] C. H. Schiller et al, *Proceedings of the 36th EUPVSEC*, p. 995–999 (2019).
[6] IEC 60891:2009–12.
[7] R. Lausch et al, *Proceedings of the 35th EUPVSEC*, p. 1060–4 (2018).
[8] D. Eberlein et al, *Practical Metallography*, Vol. 48-5, p. 239–260 (2011).
[9] IEC 61215: 2005.
[10] L. Tous et al, *Progress in Photovoltaics: Research and applications*, submitted (2022).